

**Simulation study on the trembling shear behavior of electrorheological fluid**F. Yang,<sup>1</sup> X. L. Gong,<sup>1,\*</sup> S. H. Xuan,<sup>1</sup> W. Q. Jiang,<sup>2</sup> C. X. Jiang,<sup>2</sup> and Z. Zhang<sup>3</sup><sup>1</sup>*CAS Key Laboratory of Mechanical Behavior and Design of Materials, Department of Modern Mechanics, University of Science and Technology of China (USTC), Hefei 230027, People's Republic of China*<sup>2</sup>*Department of Chemistry, USTC, Hefei 230026, People's Republic of China*<sup>3</sup>*National Center for Nanoscience and Technology, Beijing 100080, People's Republic of China*

(Received 20 December 2010; revised manuscript received 12 May 2011; published 25 July 2011)

The trembling shear behavior of electrorheological (ER) fluids has been investigated by using a computer simulation method, and a shear-slide boundary model is proposed to understand this phenomenon. A thiourea-doped Ba-Ti-O ER fluid which shows a trembling shear behavior was first prepared and then systematically studied by both theoretical and experimental methods. The shear curves of ER fluids in the dynamic state were simulated with shear rates from 0.1 to 1000 s<sup>-1</sup> under different electric fields. The simulation results of the flow curves match the experimental results very well. The trembling shear curves are divided into four regions and each region can be explained by the proposed model.

DOI: [10.1103/PhysRevE.84.011504](https://doi.org/10.1103/PhysRevE.84.011504)

PACS number(s): 83.80.Gv, 83.50.Ax, 87.55.Gh, 83.60.Np

**I. INTRODUCTION**

Electrorheological (ER) fluid, a typical smart material, is usually composed of microsized or nanosized dielectric particles dispersed in a liquid with a low dielectric constant [1–3]. When an electric field is applied, the randomly dispersed particles are rearranged along the field direction and form complex columnlike structures, resulting in a dramatic change of the apparent viscosity. The change is fast (milliseconds) and reversible, which makes ER fluids desirable for technological and industrial applications [4,5]. The remarkable increase of the viscosity of the ER fluid is caused by the formation of chains that bridge the two opposite electrodes, and the rheological properties (i.e., flow behavior) are affected by the structure transformations. Therefore, the structure transformation is fundamental in understanding the physical mechanism and properties of ER fluids. More work should be done in this area to gain more knowledge of the flow behavior of ER fluids, either by material design or computer simulation.

The macroscopic rheological properties of ER fluids are determined by the microstructure of the particles suspended in the system. Many computer simulations, which focus on linking the microscopic behavior to the macroscopic response of an ER suspension, have been reported in both the static and dynamic states. Some researchers studied the microstructure transformation of the ER fluids. Based on a static simulation, Tao and Jiang found that a body-centered-tetragonal (bct) structure was formed in the ER fluids due to the Brownian and dipolar forces, which agreed well with the experimental observations [6]. Gulley and Tao found that different structures were achieved under different Brownian-to-dipolar forces ratios [7]. Considering the shear force effect, both Melrose and Guo *et al.* developed the structural phase diagram of ER fluids [8,9]. Cao *et al.* examined the shear flow and lamellar structure of ER fluids with electric field by using computer simulation and experimental observation [10]. Besides the microstructure of ER suspensions, the macroscopic response has also attracted wide attention. Sun and Tao investigated the

viscosity of a one-component polarizable fluid under different electric field intensities, and formed the relation between the viscosity and the shear rate [11]. Similarly, Enomoto and Oba studied the viscosity of ER fluids under different electric field intensities with a large-scale simulation [12]. The properties of ER fluids in the static state were simulated considering the effect of the multipole moment by Lapenta and co-workers [13]. Klingenberg and co-workers studied the dynamic yield stress with both simulations and experiments under small shear rate response [14,15]. To date, the structure transformations and simple rheological properties of ER fluids have been particularly discussed by using computer simulations. In recent years, the trembling shear behavior, in which the shear stress increases and decreases with shear rate, has interested many researchers. This particular shear behavior, which was first introduced by Ko and co-workers [16], reflected the unique microstructure transformations in ER fluids. A lot of work has been done on the experimental study of the trembling shear behavior [16–18]. However, computer simulations focused on the trembling shear behavior have not been reported.

In this work, to systematically examine the trembling shear behavior of ER fluids, an experiment was first conducted to study the flow behavior of ER fluids, and then a subsequent computer simulation was performed to investigate the rheological properties of ER fluids. The as-prepared material showed a typical trembling shear behavior; a shear-slide boundary model is proposed to understand its mechanism. The boundary friction force is introduced into our model, and it is believed to be an important factor in influencing the properties. The simulated shear curves match the experimental results very well. Moreover, the trembling shear behavior is divided into four regions and each region can be explained by the proposed model.

**II. EXPERIMENT**

The ER fluid used in this experiment was made of thiourea-doped Ba-Ti-O particles in silicone oil. Two suspensions were made with weight fractions of 5 and 15 wt% (thiourea to particles). The average size of the particles which were prepared by a sol-gel method is 5 μm. The viscosity and

\*gongxl@ustc.edu.cn

the dielectric constant of silicone oil are 0.1 Pa·s and 2.6, respectively. The volume fraction is 30%. The rheological behavior of the suspension was investigated by a rotational rheometer (Physica MCR 301, Anton Paar), ER HVS/ERD 180, and the CC10-E accessory.

### III. MODEL AND SIMULATION

The ER system which is simulated in this paper consists of  $N$  spherical particles (the relative dielectric constant is  $\varepsilon_p$  and the diameter is  $\sigma$ ) suspended in a silicone oil fluid whose relative dielectric constant and viscosity are  $\varepsilon_f$  ( $\varepsilon_f < \varepsilon_p$ ) and  $\eta_f$ , respectively. The tested ER fluid which is confined between two parallel-plate electrodes is separated by a distance  $L_z$ . An external electric field is applied perpendicularly to the parallel plate (the  $z$  direction), and a steady shear rate  $\dot{\gamma}$  is imposed along the  $x$  direction (parallel with the plate). Here, the velocity field is varied linearly along the  $z$  direction (the top electrode moves at a speed of  $\dot{\gamma}L_z$ ). Before the application of the electric field, particles are randomly dispersed in the medium fluid. When the electric field  $E_0$  is applied in the  $z$  direction, each particle gets an induced dipole moment  $\mathbf{p} = (1/2)\pi\beta\varepsilon_0\varepsilon_f\sigma^3\mathbf{E}_{\text{loc}}$  in the fluid with relative dielectric constant  $\varepsilon_f$  (in the SI unit system), where  $\beta = (\varepsilon_p - \varepsilon_f)/(\varepsilon_p + 2\varepsilon_f)$  and  $\mathbf{E}_{\text{loc}}$  is the local field, with  $\mathbf{E}_{\text{loc}} = E_0\hat{z}$  if  $\beta \ll 1$ . The orientational relaxation of the induced dipoles and the chain effect on the motion of the dispersing fluid are not considered in this model. The particles are not free to rotate, and the dipole moment is considered always parallel to the electric field. The motion of the  $i$ th particle is described by [9]

$$m d^2 \mathbf{r}_i / dt^2 = \mathbf{F}_i - 3\pi\sigma\eta_f(d\mathbf{r}_i/dt - \dot{\gamma}z_i\hat{x}) + \mathbf{R}_i, \quad (1)$$

where  $m$  is the mass of particles and  $\mathbf{r}_i$  is the position of the  $i$ th particle at time  $t$ . The first term  $\mathbf{F}_i$  is the interparticle force, the second is the Stokes drag, and the third is the Brownian force. The dipolar force acting on the  $i$ th particle from the particle at  $r_j$  is given by

$$\mathbf{F}_{ij}^{\text{el}} = F_0(\sigma/r_{ij})^4[(1 - 3\cos^2\theta_{ij})\hat{r} - \sin(2\theta_{ij})\hat{\theta}], \quad (2)$$

where  $p = |\mathbf{p}|$ ,  $\mathbf{r}_{ij} = r_i - r_j$  with  $r_{ij} = |\mathbf{r}_{ij}|$ ,  $\theta_{ij}$  is the angle between  $\mathbf{r}_{ij}$  and the  $z$  axis,  $\hat{r} = \mathbf{r}_{ij}/r_{ij}$ , and  $F_0 = 3p^2/(4\pi\varepsilon_0\varepsilon_f\sigma^4)$ . To simulate interactions between the hard spheres and the interactions between the hard sphere and the hard wall (the two electrodes), an exponential short-range repulsive force between particles  $i$  and  $j$  is introduced:

$$\mathbf{F}_{ij}^{\text{rep}} = 2F_0(\sigma/r_{ij})^4 \exp[-100(r_{ij}/\sigma - 1)]\hat{r}, \quad (3)$$

and between the particle  $i$  and the hard wall:

$$\begin{aligned} \mathbf{F}_i^{\text{wall}} = & 2F_0(\sigma/z_i)^4 \exp[-100(r_{ij}/\sigma - 0.5)]\hat{z} \\ & - 2F_0[\sigma/(L_z - z_i)]^4 \exp\{-100[(L_z - z_i)/\sigma - 0.5]\}\hat{z}. \end{aligned} \quad (4)$$

Then  $\mathbf{F}_i$  is given by

$$\mathbf{F}_i = \sum_{j(j \neq i)} (\mathbf{F}_{ij}^{\text{el}} + \mathbf{F}_{ij}^{\text{rep}}) + \sum_j \mathbf{F}_{ij}^{\text{el,im}} + \mathbf{F}_i^{\text{wall}}. \quad (5)$$

where  $\mathbf{F}_{ij}^{\text{el,im}}$  is the summation force on the particle  $i$  due to an infinite number of images of particle  $j$  reflected about the elec-

trodes. The Brownian force  $\mathbf{R}_i$  is determined independently by a normal distribution with  $\langle R_{i,\alpha} \rangle = 0$  and  $\langle R_{i,\alpha}(0)R_{i,\beta}(t) \rangle = 6\pi k_B T \sigma \eta_f \delta_{\alpha\beta} \delta(t)$ .  $k_B$  is Boltzmann's constant and  $T$  is the absolute temperature. To study the parametric properties of many different ER fluids, we define dimensionless quantities to scale Eq. (1):  $\mathbf{r}_i^* = \mathbf{r}_i/\sigma$ ,  $t^* = t/[3\pi\eta_f\sigma^3/(k_B T)]$ ,  $\mathbf{R}_i^* = \mathbf{R}_i/(k_B T/\sigma)$ , and  $\mathbf{F}_i^* = \mathbf{F}_i/[p^2/(\varepsilon_0\varepsilon_f\sigma^4)]$ , so Eq. (1) can be rewritten as

$$A d^2 \mathbf{r}_i^* / dt^{*2} = Q \mathbf{F}_i^* - d\mathbf{r}_i^* / dt^* + 8\text{Pe} z_i^* \hat{x} + \mathbf{R}_i^*, \quad (6)$$

where  $Q = p^2/(\varepsilon_0\varepsilon_f\sigma^3 k_B T)$  and  $\text{Pe} = 3\pi\eta_f\sigma^3 \dot{\gamma}/(8k_B T)$ . For the ER fluids, the magnitude of  $A = mk_B T/(3\pi\eta_f\sigma^2)^2$  in Eq. (6) is very small ( $\sim 10^{-10}$ ), so this inertial effect is neglected in the following simulations. Thus, it is simplified as

$$d\mathbf{r}_i^* / dt^* = Q \mathbf{F}_i^* + 8\text{Pe} z_i^* \hat{x} + \mathbf{R}_i^*. \quad (7)$$

Equation (7) is integrated with a time step  $\Delta t^* \leq 0.01/(F_{\text{max}}^* Q)$  using Euler's method;  $F_{\text{max}}^*$  is the dimensionless maximum interparticle force acting on particles, thus the maximum displacement of particles cannot exceed  $0.01\sigma$ .

In this work, a system of  $N = 300$  particles in a box with  $L_x = 10\sigma$ ,  $L_y = 5\sigma$ ,  $L_z = 10\sigma$  is simulated. The particle volume fraction is 0.3. Periodic boundary conditions are imposed in the  $x$  and  $y$  directions; reflecting boundary conditions and the shear-slide boundary model are in the  $z$  direction.

The shear-slide boundary model is proposed to understand the mechanism of the trembling shear behavior of the ER fluids. Here, the effect of the boundary friction force between the boundary particles and the electrodes is considered. The boundary friction force which has been discussed in many works is believed to be an important factor in influencing the rheological properties of the ER and magnetorheological (MR) fluids [19,20]. When the electric field is applied to the ER fluids, the induced dipoles lead to a long-range interaction that causes the particles to rearrange to form a chainlike structure along the field direction. As soon as a shear is applied, the chains tilt in the direction of shear. We attribute the chains' inclination to  $x$ -direction forces, which may respond to the viscous force and the friction force between the chains and the electrodes. The friction force between the chains and the electrodes are attributed to the chains' inclination. To get a clear understanding of the effect of the boundary friction force, the force analysis is done on the boundary particles that adhered to the electrodes.

The boundary particles are the particles that have adhered to the electrodes. When particles are close enough to the electrodes ( $< 0.55\sigma$ , from the center of particle to the electrodes), the particles are defined to be adhered to the electrodes (they only move in the  $x$  and  $y$  directions, not in the  $z$  direction). Without slipping (between the chains and the electrodes; Fig. 1), the forces which acted on the boundary particles can be written as

$$F_{\text{fric}} - 3\pi\sigma\eta_f\dot{\gamma}[L_z - (L_z - \sigma/2)] - f_r \sin\theta - f_\theta \cos\theta = 0, \quad (8)$$

$$F_{\text{fric}} - 3\pi\sigma\eta_f\dot{\gamma}\sigma/2 - f_r \sin\theta - f_\theta \cos\theta = 0, \quad (9)$$

where  $F_{\text{fric}}$  is the friction force between the chains and the electrodes. Because no slip occurs between the chains and the

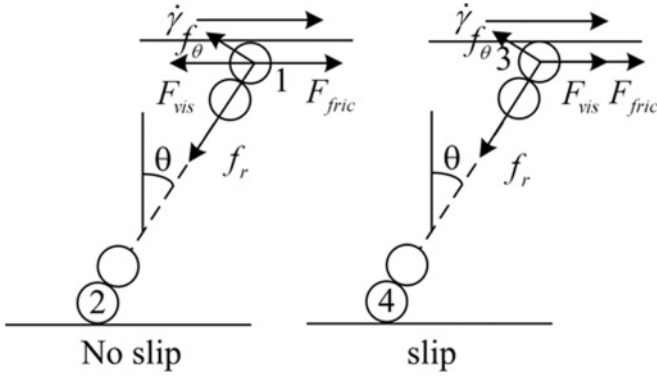


FIG. 1. Schematic representation of the shear-slide model.

electrodes,  $-F_{s,\text{fric}} \leq F_{\text{fric}} \leq F_{s,\text{fric}}$ , and  $F_{s,\text{fric}}$  is the biggest static friction force. The second term is the expression of  $F_{\text{vis}}$ , and  $f_r$  is the  $\hat{r}$  component of the dipole force;  $f_\theta$  is the  $\hat{\theta}$  component of the dipole force acting on the boundary particles. Without slipping, the boundary particles adhere to the top electrodes and the bottom electrodes move at a speed of  $\dot{\gamma}L_z$  and 0 separately. Equations (8) and (9) have the same result but with different expressions. So from Eq. (8) the tilt angle  $\theta$  as a function of  $F_{\text{fric}}$  and the  $\dot{\gamma}$  is obtained as

$$\theta = \sin^{-1} \frac{(F_{\text{fric}} - 3\pi\sigma\eta_f\dot{\gamma}\sigma/2)}{\sqrt{f_\theta^2 + f_r^2}} - \alpha, \quad (10)$$

with  $\tan \alpha = \frac{f_\theta}{f_r}$ .

If  $F_{\text{fric}} = F_{s,\text{fric}}$ , the biggest tilt angle  $\theta_c$  is obtained (in the no slip state). Here,  $\theta_b$  is defined as the angle at which the chains will break. If the friction force  $F_{s,\text{fric}}$  obtains the value where  $\theta_c$  is larger than  $\theta_b$ , the chains break before the boundary particles slip along the  $x$  direction. These simulation results are shown in Fig. 4(a). If  $F_{s,\text{fric}}$  is not big enough,  $\theta_c$  is smaller than  $\theta_b$ , and slipping will occur between the chains and the electrodes before the chains break. For the boundary particles with slipping, the forces acting on particles can be written as

$$F_{\text{fric}} + 3\pi\sigma\eta_f[\dot{\gamma}(L_z - \sigma/2) - v_3] - f_r \sin \theta - f_\theta \cos \theta = 0, \quad (11)$$

$$F_{\text{fric}} + 3\pi\sigma\eta_f[v_4 - \dot{\gamma}\sigma/2] - f_r \sin \theta - f_\theta \cos \theta = 0, \quad (12)$$

where  $F_{\text{fric}} = F_{d,\text{fric}}(\dot{\gamma})$ ;  $F_{d,\text{fric}}(\dot{\gamma})$  is the dynamic friction force and the second term is the viscous force. When the angle reaches  $\theta_c$ , the boundary particles slip and the dynamic friction force and the viscous force make the chains tilt in the direction of the shear force. The tilt angle does not increase until  $v_3$  and  $v_4$  are equal.  $v_3$  and  $v_4$  are the velocities of particles 3 and 4, respectively. Therefore a stable tilt angle  $\theta_s$  is obtained from Eqs. (11) and (12) with  $v_3 = v_4$ :

$$\theta_s = \sin^{-1} \frac{[F_{d,\text{fric}}(\dot{\gamma}) + 3\pi\sigma\eta_f\dot{\gamma}(L_z/2 - \sigma/2)]}{\sqrt{f_\theta^2 + f_r^2}} - \alpha, \quad (13)$$

$$\text{and } v_3 = v_4 = \dot{\gamma}L_z/2.$$

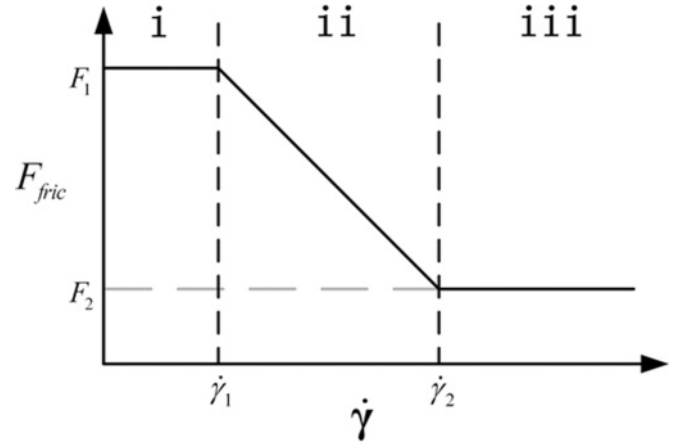


FIG. 2. Schematic representation of friction force against shear rate.

The dynamic friction force  $F_{d,\text{fric}}$  is taken as a function of  $\dot{\gamma}$  [21], and a simple relation is shown in Fig. 2. In region i, no slip occurred between the boundary particles and the electrodes. The friction force is equal to the static friction force. In region ii, with increasing shear rate, the dynamic friction force transforms to a sliding friction force, and then is further coupled with a rolling friction force. The lubricated friction may also play a part in it. In region iii, the friction force is mainly composed of rolling friction force and lubricated friction force, and is much smaller than the static friction force. According to experimental data in Fig. 5,  $\dot{\gamma}_1 = 0.1$  and  $\dot{\gamma}_2 = 5$ . In this simulation,  $F_1 = 0.08F_0$  and  $F_2 = F_1/10$  were assumed.

In the dynamic state, rheological properties are determined by the effective viscosity  $\eta_{\text{eff}}$ , which can be calculated from the stress  $\tau_{zx}$  ( $\eta_{\text{eff}} = \langle \tau_{zx} \rangle / \dot{\gamma}$ ). The  $\tau_{zx}$  is the  $zx$  component of the stress tensor, which is an averaged value of the simulations. By using the Bingham model,  $\tau_{zx}$  is expressed as  $\tau_{zx} = \tau_E + \eta_s \dot{\gamma}$ , where  $\eta_s$  is the viscosity of suspensions (without electric field). The  $\eta_s$  is expressed as  $\eta_s = \eta_f \exp[2.5\varphi/(1 - \varphi/0.74)]$ .  $\varphi$  is the volume fraction of ER fluid;  $\varphi = 30\%$  [22]. In order to definitely understand the relationship of the particle interactions, we focused on the electric field induced shear stress  $\tau_E$ , which was calculated by Eq. (14) [23]:

$$\tau_E = \left\langle -\frac{1}{V} \sum_{i=1}^N (\mathbf{r}_i)_z (\mathbf{F}_i^{\text{el}})_x \right\rangle. \quad (14)$$

#### IV. RESULTS AND DISCUSSION

To compare the simulation results with the experimental results, some parameters are defined as follows:  $T = 300$  K,  $\varepsilon_p = 100$ ,  $\varepsilon_f = 2.6$ ,  $\sigma = 5 \mu\text{m}$ ,  $\eta_f = 0.1$  Pa·s, and  $\eta_s = 0.35$  Pa·s. The relative shear stress is expressed as  $\tau_E/\tau_0$ , where  $\tau_E$  is the electric field induced shear stress and  $\tau_0$  is the shear stress of ER fluid without electric field at the lowest shear rate.

The relation between the relative shear stress and the shear strain in the quasistatic state is shown in Fig. 3. Upon application of the electric field, the randomly dispersed particles rapidly form a chainlike structure. When the strain

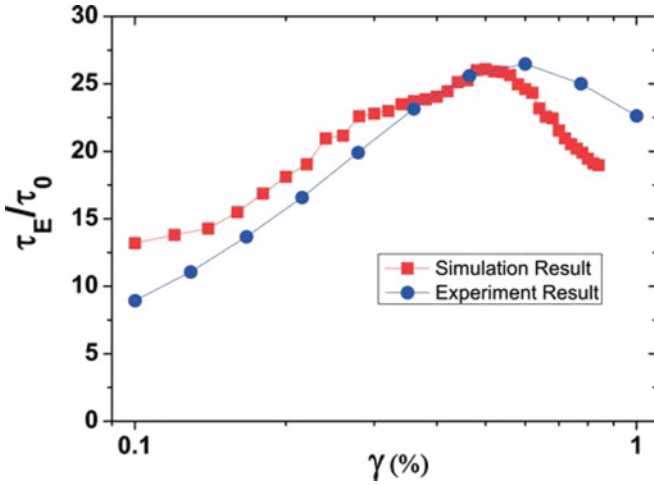


FIG. 3. (Color online) Simulation result and experimental result of relative shear stress versus shear strain in quasistatic state, with  $E = 2000$  V/mm. Simulation result is carried out at  $\dot{\gamma} = 10^{-3} \text{ s}^{-1}$ .

is less than a critical value, which is the shear yield point, the chains are kept intact. If returned to the unstrained state, these chains appear unaffected. In that state, the suspension appears like an elastic solid; it is assumed that no slip occurred between the boundary particles and the electrode. The simulation result in Fig. 3 is carried out under the condition of  $\dot{\gamma} = 10^{-3} \text{ s}^{-1}$  and no slip occurs between the boundary particles and the electrodes. In comparison to the experimental result, the simulation shows a typical shear stress-shear strain relation (Fig. 3).

Here, the effect of the boundary friction force on the relative shear stress is examined Fig. 4 shows the dependency of time on the variation of relative shear stress in different friction boundary conditions: In Fig. 4(a), the boundary friction force acting on the boundary particles is so big that no slip occurs between the boundary particles and the electrodes. Under the electric field and shear flow, the particles aggregate to form chains and tilt in the shear direction. The chain structure tilts to the angle where the yield occurs, where the relative shear stress becomes the largest. Beyond the yield point the chains cannot remain intact, so a less relative shear stress is obtained. The structure ruptured and went through a reformation process when the relative shear stress went up and down [24]. It can also be seen from Fig. 4(a) that the peak value of the relative shear stress increases with time. More through chains often lead to a higher yield stress. In this situation, the perturbation of relative shear stress is so large that the relative shear stress cannot be chosen as the value in the flow curves to compare with experimental data. In Fig. 4(b), the friction force is not large enough for the chain tilt angle to reach the structure-break angle  $\theta_b$ . Chains tilt to the critical angle  $\theta_c$  where the boundary particles slide along the electrodes, as expressed by Eq. (9). Then, under the application of the dynamic friction force and the Stokes force, the chain tilt angle maintains at a stable state where the tilt angle is  $\theta_s$  [as shown in Eq. (12)]. In this case, the perturbation of shear stress is much smaller than that in Fig. 4(a). The stable relative shear stress can be used as the value in the flow curves to compare with the experimental data. In Fig. 4(c), the friction force is zero, the Stokes drag

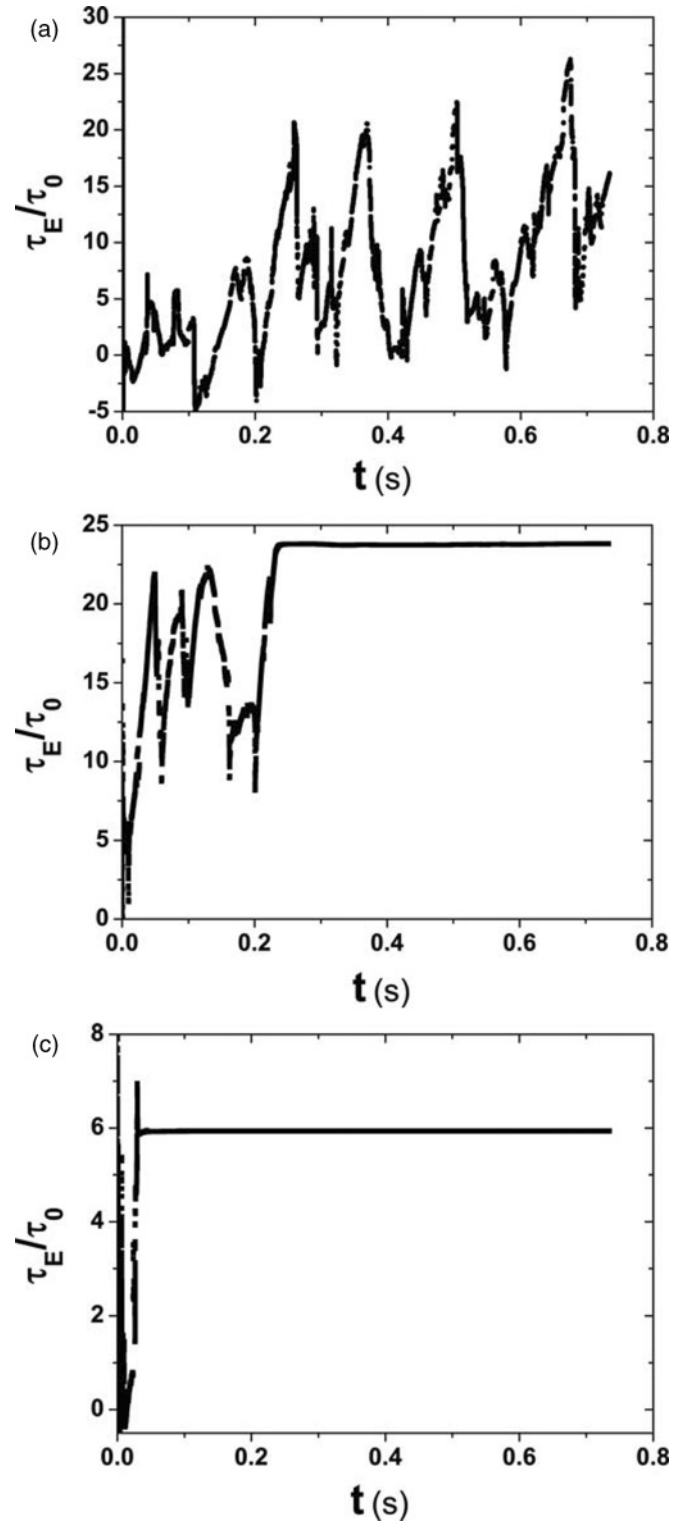


FIG. 4. Shear stress versus time,  $E = 2$  kV/mm,  $\dot{\gamma} = 0.1 \text{ s}^{-1}$ . (a) The boundary friction force is large enough that no slip occurs between the boundary particles and electrodes. (b) A moderate boundary friction force is chosen; the boundary particles do not slide when forces acting on the boundary particles are smaller than the friction force. Boundary particles slide when forces acting on the particles are large than the friction force. (c) The boundary friction force is zero, so particles cannot adhere to electrodes.

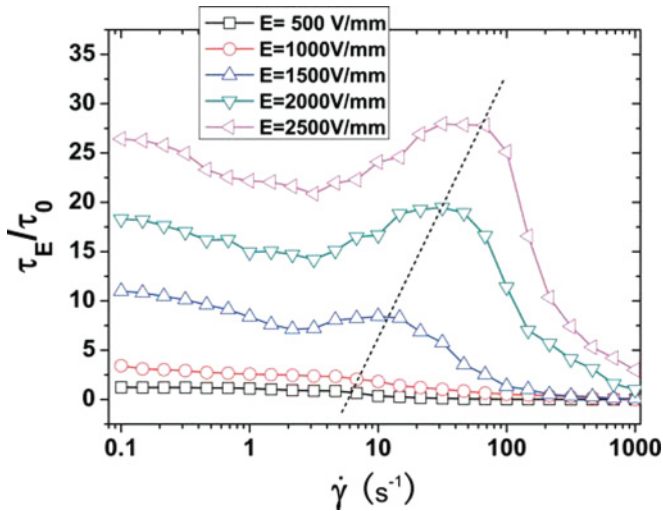


FIG. 5. (Color online) Simulation results of relative shear stress versus shear rate at different electric fields.

force leads to a small tilt angle, and the relative shear stress remains nearly constant. The three situations are discussed under typical friction force. Some intermediate states exist between the three states. Between the states in Figs. 4(a) and 4(b), the relative shear stress has a perturbation smaller than in Fig. 4(a) and larger than in Fig. 4(b). The tilt angle fluctuates along the stable angle with the relative shear stress ups and downs. When the state in Fig. 4(b) gradually turns into that in Fig. 4(c), the boundary friction force becomes smaller, yielding smaller relative shear stress. This may occur where the boundary friction force turns from region II into region III in Fig. 2.

In order to obtain the flow curve, the shear stresses  $\tau$  were calculated at a series of shear rates from 0.1 to 1000  $\text{s}^{-1}$  (6 points every order of magnitude, and totally 25 points every curves). The interval between the points is so small that the simulation flow curves can be considered to be applicable to a continuous shear flow, which is similar to the experimental testing. The relative shear stress is expressed as  $\tau_E/\tau_0$ , where  $\tau_E$  is the electric field induced shear stress,  $\tau_E = \tau|_{E \neq 0} - \tau|_{E=0}$ , and  $\tau_0$  is the shear stress of ER fluid at the smallest shear rate without applying an electric field. Figure 5 shows the simulation results of relative shear stress versus shear rate under different electric fields. The shear rate increases step by step. Each shear stress data point at a certain shear rate in Fig. 5 is calculated separately. The data are obtained by choosing the stable relative shear stress at a given electric field and shear rate [in Fig. 4(b)]. Figure 6 shows the original experimental data of flow curves, and Fig. 7 is the transformed data of flow curves of the thiourea-doped Ba-Ti-O ER fluid tested at different electric fields.

As shown in Fig. 6, it is very clear that the as-prepared ER fluids show a trembling shear behavior, which has been introduced in previous reports [16–18]. As the electric field is increased, the trembling shear behavior becomes more obvious. The trembling flow curves can be divided into four regions and this behavior can be explained by using the proposed shear-slide model. In region I, the shear stress decreases with increase of the shear rate (Fig. 6). As soon as

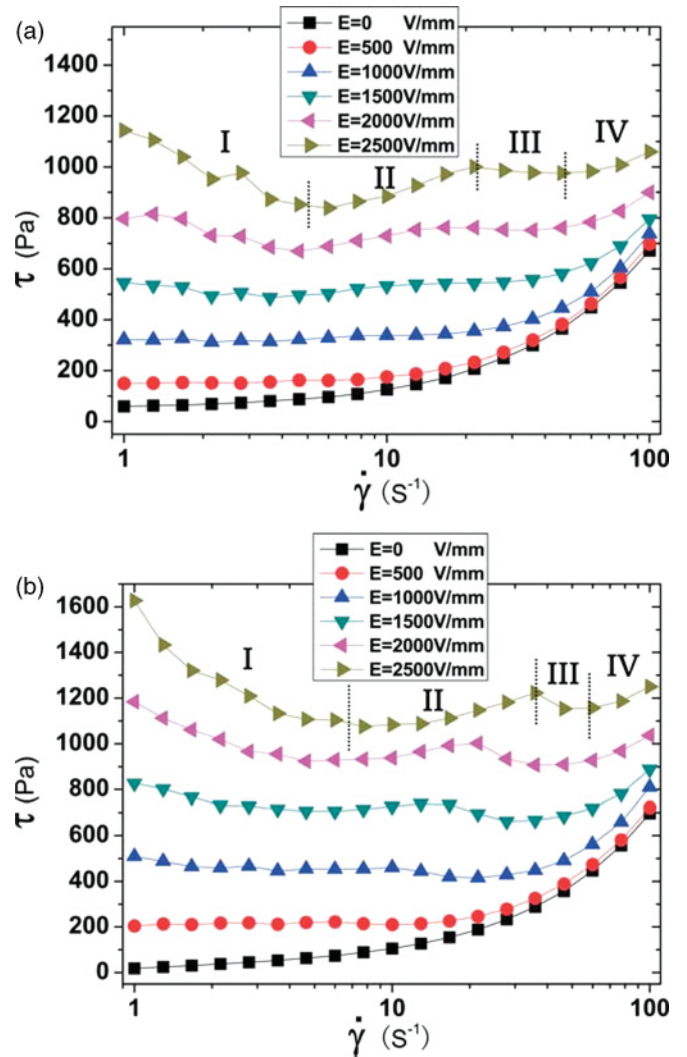


FIG. 6. (Color online) Original experimental results of shear stress versus shear rate at different electric fields. (a) 5 wt% thiourea-doped Ba-Ti-O ER fluid; (b) 15 wt% thiourea-doped Ba-Ti-O ER fluid.

the shear force is applied, ER fluid transforms to the elastic solid state and the yield stress is obtained as the shear stress. With increase of the shear rate, ER fluid flows along the direction of shear force, and both the breakage of the chains and slip occur between the chains and the electrodes. The chains' rupture will cause the shear stress to decrease. The slipping between the chains and the electrodes also plays a part in the decrease of the shear stress. From Eq. (13) it is found that the tilt angle of the chains is a function of dynamic boundary friction force and shear rate. When the shear rate increases, the dynamic boundary friction force decreases and the viscous force increases. However, the increment is smaller than the decrement in region I, thus the tilt angle decreases with increase of the shear rate in region I. A small tilt angle means a small shear stress, so a small shear stress is obtained. Region II shows a typical ER curve of shear stress against shear rate. In this region, the dynamic boundary friction force is nearly constant, and the viscous force increases, so the shear stress increases with increase of the shear rate from Eq. (13).

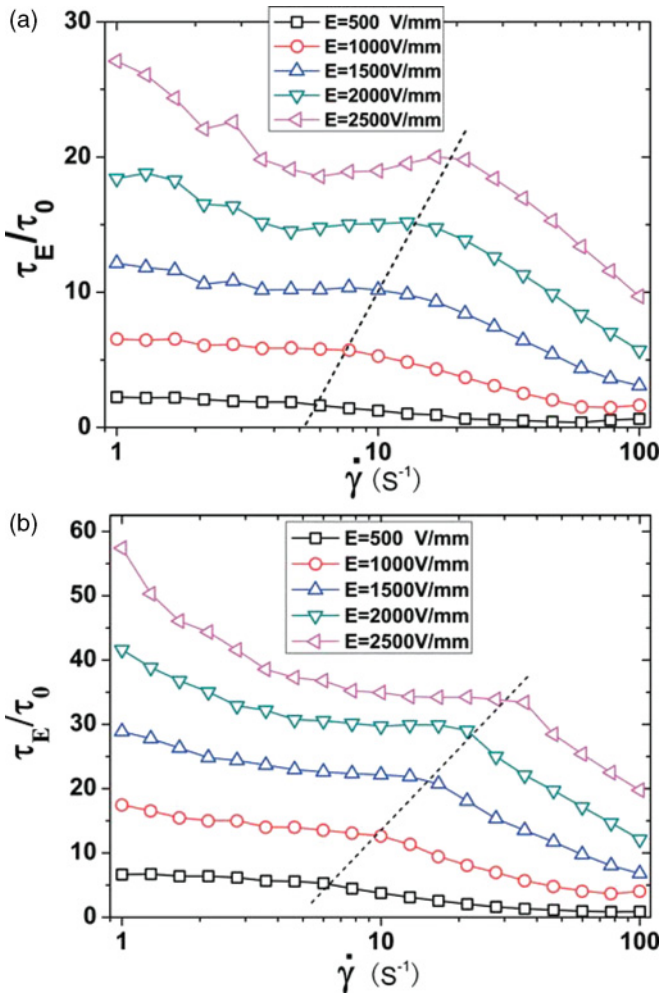


FIG. 7. (Color online) Transformed experimental results of relative shear stress versus shear rate at different electric fields. (a) 5 wt% thiourea-doped Ba-Ti-O ER fluid; (b) 15 wt% thiourea-doped Ba-Ti-O ER fluid.

In region III, the shear stress decreases with increase of the shear rate. From Figs. 5 and 7, it is found that the relative shear stress reduces to zero in region III, because the shear field is strong enough to counteract the electric field and the ordered chainlike structures cannot be formed to give a strong shear stress. Here, the shear stress decreases below a certain shear rate. This shear rate, which is defined as the break shear rate, is correlated to the electric field. Experimental results and simulation results both indicate that the break shear rate is linearly dependent on the square of the electric field (Fig. 8). The Stokes force is proportional to the shear rate, and the dipolar force is proportional to  $E^2$ . Therefore, it is found that the shear force is linearly dependent on the dipolar force at break shear rate. Figure 6 shows that a larger electric field often leads to a more obvious trembling behavior. According to Eq. (13), the larger break shear rate is obtained under a larger electric field, and a larger shear rate leads to larger shear stress. Thus the trembling phenomenon becomes more obvious under a larger electric field. In region IV, the contribution of shear stress is dominated by  $\eta\dot{\gamma}$  according to the Bingham equation  $\tau = \tau_E + \eta\dot{\gamma}$ , and the electric field induced shear stress is much smaller than that. In this situation, the effect

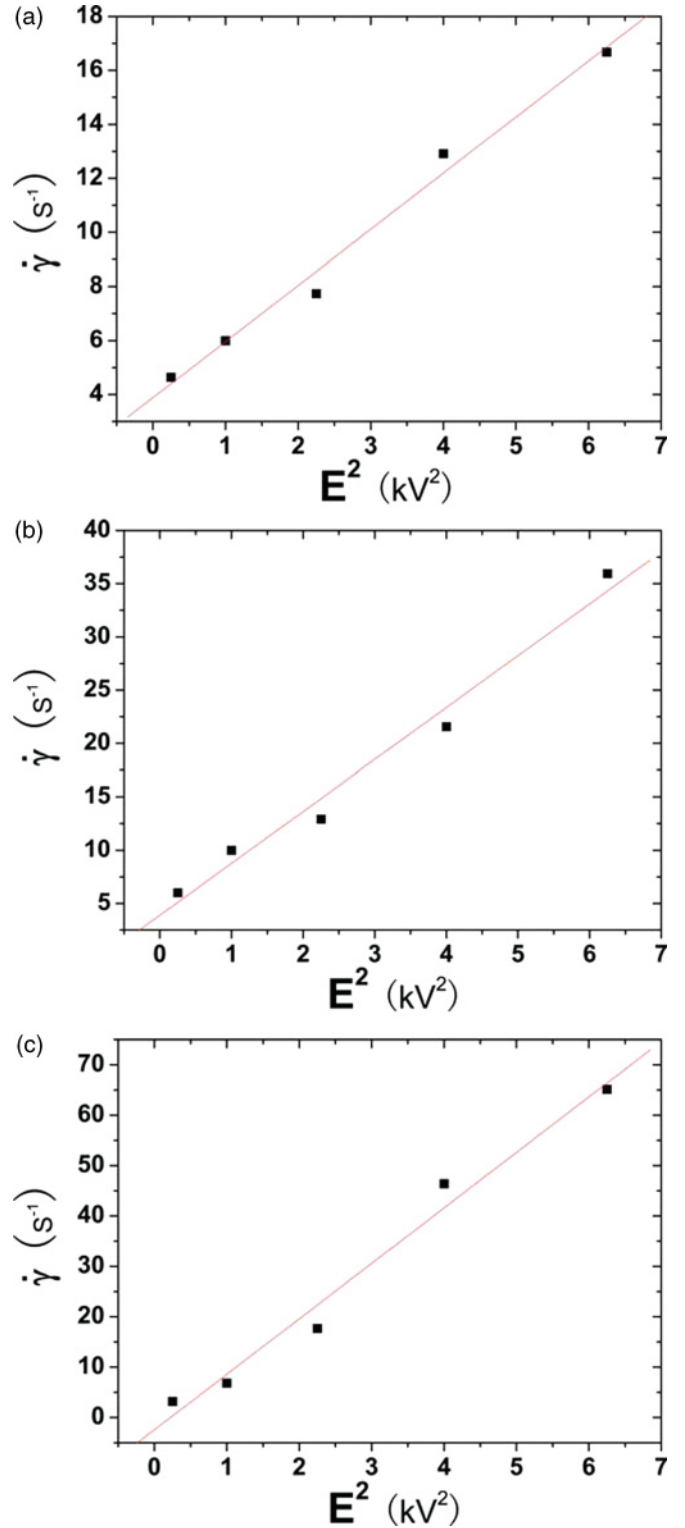


FIG. 8. (Color online) The relation of the square of the electric field and the break shear rate. (a) 5 wt% thiourea-doped Ba-Ti-O ER fluid; (b) 15 wt% thiourea-doped Ba-Ti-O ER fluid; (c) Simulation results.

of the electric field is much smaller than that of shear; a chainlike structure is formed in the  $x$  direction rather than in the  $z$  direction. Thus, the shear stress increases with increase of the shear rate in region IV.

## V. CONCLUSIONS

The trembling shear behavior of ER fluids is investigated by using both simulations and experimental testing. The thiourea-doped Ba-Ti-O ER fluid shows a typical trembling shear behavior and the simulation results match well with the experimental characterization. A shear-slide boundary model considering the boundary frictional force is proposed to discuss this phenomenon. The trembling shear behavior is divided into four regions. In region I, shear stress decreases with increase of the shear rate, due to the breakage of the chains and the boundary friction force which decreases with increase of the shear rate. In region II, shear stress increases with increase of the shear rate, which is because the shear stress is proportional to shear rate and the boundary friction force shows only a little effect on the shear stress in this region. In region III, shear stress decreases with increase of the shear rate. The shear field is strong enough to counteract the electric field, so ordered

structures cannot be formed to give a strong shear stress. In region IV, the electric field induced shear stress is negligible and the  $\eta\dot{\gamma}$  shows a dominant effect on the shear stress.

Both the electric field and the shear field play major roles in controlling the particle movement in this simulation. The electric field forces particles to form chains, while the shear field destroys them. Therefore, the shear stress is highly influenced by the two introduced fields. In addition, the rheological properties are greatly affected by the boundary friction force between the electrodes and the chain structures, which can be used to investigate the shear behavior of ER fluids more precisely.

## ACKNOWLEDGMENTS

Financial support from National Basic Research Program of China (973 Program, Grant No. 2007CB936800) is gratefully acknowledged.

- 
- [1] T. C. Halsey, *Science* **258**, 761 (1992).
  - [2] W. J. Wen, X. X. Huang, S. H. Yang, K. Q. Lu, and P. Sheng, *Nat. Mater.* **2**, 727 (2003).
  - [3] W. Q. Jiang, C. X. Jiang, X. L. Gong, and Z. Zhang, *J. Sol-Gel Sci. Technol.* **52**, 8 (2009).
  - [4] R. Tao and J. M. Sun, *Phys. Rev. Lett.* **67**, 398 (1991).
  - [5] J. R. Melrose, *Phys. Rev. A* **44**, R4789 (1991).
  - [6] R. Tao and Q. Jiang, *Phys. Rev. Lett.* **73**, 205 (1994).
  - [7] G. L. Gulley and R. Tao, *Phys. Rev. E* **56**, 4328 (1997).
  - [8] J. R. Melrose, *Mol. Phys.* **76**, 635 (1992).
  - [9] H. X. Guo, Z. H. Mai, and H. H. Tian, *Phys. Rev. E* **53**, 3823 (1996).
  - [10] J. G. Cao, J. P. Huang, and L. W. Zhou, *J. Phys. Chem. B* **110**, 11635 (2006).
  - [11] J. M. Sun and R. Tao, *Phys. Rev. E* **52**, 813 (1995).
  - [12] Y. Enomoto and K. Oba, *Phys. A* **309**, 15 (2002).
  - [13] G. Lapenta, G. Maizza, A. Palmieri, G. Boretto, and M. Debenedetti, *Phys. Rev. E* **60**, 4505 (1999).
  - [14] D. J. Klingenberg, F. Vanswol, and C. F. Zukoski, *J. Chem. Phys.* **94**, 6160 (1991).
  - [15] D. J. Klingenberg, F. Vanswol, and C. F. Zukoski, *J. Chem. Phys.* **94**, 6170 (1991).
  - [16] Y. G. Ko, U. S. Choi, and Y. J. Chun, *Macromol. Chem. Phys.* **209**, 890 (2008).
  - [17] Y. G. Ko, U. S. Choi, and Y. J. Chun, *J. Colloid Interface Sci.* **335**, 183 (2009).
  - [18] J. B. Yin, X. Xia, L. Q. Xiang, Y. P. Qiao, and X. P. Zhao, *Smart Mater. Struct.* **18**, 095007 (2009).
  - [19] L. Ren and K. Q. Zhu, *Smart Mater. Struct.* **15**, 1794 (2006).
  - [20] Y. Pappas and D. J. Klingenberg, *Rheol. Acta* **45**, 621 (2006).
  - [21] B. Bhushan, *Introduction to Tribology* (John Wiley & Sons, New York, 2002).
  - [22] M. Mooney, *J. Colloid Sci.* **6**, 162 (1951).
  - [23] Z. H. Sun, X. X. Wang, A. K. Soh, and H. A. Wu, *Modell. Simul. Mater. Sci. Eng.* **14**, 423 (2006).
  - [24] D. J. Klingenberg and C. F. Zukoski, *Langmuir* **6**, 15 (1990).